

Development of photoactive Sweet-C₆₀ for pancreatic cancer stellate cell therapy

Maciej Serda^{‡,1,2}, Matthew J Ware^{‡,3}, Jared M Newton^{3,4,5}, Sanchit Sachdeva³, Martyna Krzykawska-Serda^{3,6}, Lam Nguyen³, Justin Law³, Andrew O Anderson³, Steven A Curley^{1,3,7}, Lon J Wilson^{*,1} & Stuart J Corr^{*,1,3,8,9}

¹Department of Chemistry & Smalley-Curl Institute, Rice University, Houston, TX 77251, USA

²Institute of Chemistry, University of Silesia in Katowice, Katowice, 40-006, Poland

³Michael E. DeBakey Department of Surgery, Baylor College of Medicine, Houston, TX 77030, USA

⁴Department of Otolaryngology-Head & Neck Surgery, Baylor College of Medicine, Houston, TX 77030, USA

⁵Interdepartmental Graduate Program in Translational Biology & Molecular Medicine, Baylor College of Medicine, Houston, TX 77030, USA

⁶Faculty of Biochemistry, Biophysics & Biotechnology, Jagiellonian University, Kraków, 30-387, Poland

⁷Department of Mechanical Engineering & Materials Science, Rice University, Houston, TX 77005, USA

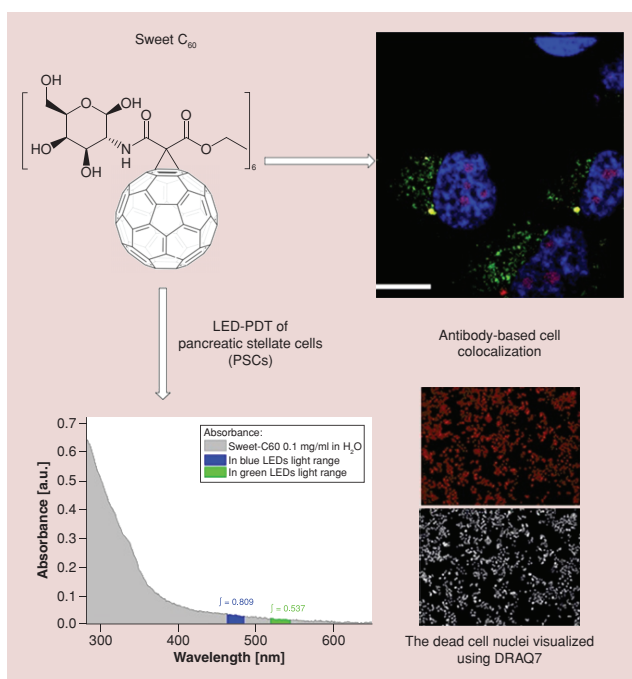
⁸Department of Biomedical Engineering, University of Houston, Houston 77204, TX, USA

⁹School of Medicine, Swansea University, Swansea, Wales, SA2 8PP, UK

*Author for correspondence: Tel.: +17 137 983 227; scorr@bcm.edu

‡Authors contributed equally

Aim: Glycoconjugated C₆₀ derivatives are of particular interest as potential cancer targeting agents due to an upregulated metabolic glucose demand, especially in the case of pancreatic adenocarcinoma and its dense stroma, which is known to be driven by a subset of pancreatic stellate cells. **Materials & methods:** Herein, we describe the synthesis and biological characterization of a hexakis-glucosamine C₆₀ derivative (termed 'Sweet-C₆₀'). **Results:** Synthesized fullerene derivative predominantly accumulates in the nucleus of pancreatic stellate cells; is inherently nontoxic up to concentrations of 1 mg/ml; and is photoactive when illuminated with blue and green light, allowing its use as a photodynamic therapy agent. **Conclusion:** Obtained glycoconjugated nanoplatform is a promising nanotherapeutic for pancreatic cancer.



First draft submitted: 11 July 2018; Accepted for publication: 4 October 2018; Published online: 3 December 2018

Keywords: [60]fullerene • fullerene antibody • glycoconjugates • pancreatic stellate cells • photodynamic therapy

The [60]fullerene molecule (C_{60}) has unique physicochemical properties [1,2], and it can be considered to bridge the gap between molecules and nanoparticles due to its small size (~ 1 nm diameter). A myriad of available surface modifications allows C_{60} to be tuned for specific biomedical applications [3] such as photodynamic therapy (PDT) agents [4,5], drug-delivery vehicles [6], transfection agents [7], MRI contrast agents [8], antimicrobials [9] and antioxidants [10].

We have previously shown that C_{60} derivatives can be used as convenient scaffolds for anticancer therapeutic drug delivery [11], and that such agents preferentially localize in both the intracellular nuclear pore complex [12] and tumor vasculature [13]. Other applications investigated in our labs include the use of C_{60} derivatives to enhance noninvasive radiofrequency cancer therapy [14–16] and to serve as efficacious MRI contrast agents [17–19].

In addition, glycoconjugated [60]fullerenes have been investigated for enhanced cancer-targeting properties [20–22]. This is because cancer cells have an increased demand for glucose, which is then metabolized at a higher rate in order to generate the energy that is necessary for many features of cancer cell proliferation and tumorigenesis [23,24]. Additionally, the family of glucose transporter membrane proteins (GLUTs) are overexpressed in several cancers including pancreatic cancer [25,26], making them an attractive molecular target for many drugs [27]. This is especially prevalent in pancreatic ductal adenocarcinoma (PDAC), which is an ideal target for glycoconjugated C_{60} therapy as reports have shown PDAC to possess increased glucose consumption via the detection of ^{18}F -deoxyglucose accumulation due to overexpression of GLUT transporters [28]. An important cellular subcomponent of PDAC tumors are pancreatic stellate cells (PSCs). Activated PSCs are known to drive the dense stromal reaction often found in human pancreatic tumors [29]. Recent studies, including those performed in our labs [30], have alluded to PSCs playing an important role in PDAC progression [31–36]. Hence, novel PSC targeting techniques and mechanisms have been hypothesized to play a vital role in PDAC treatment.

Herein, we report the synthesis and application of a highly water-soluble glycofullerene as a novel, PSC-targeted therapeutic agent. Specifically, we describe the synthesis and characterization of a hexakis-glucosamine C_{60} derivative (termed ‘Sweet- C_{60} ’), which predominantly accumulates in the nucleus of PSC cells, are inherently nontoxic up to concentrations of 1 mg/ml, and is also photoactive when illuminated with blue and green light, allowing it to be used as a PDT agent.

Materials & methods

Synthesis of glycofullerenes & their malonic precursors

All compounds used were reagent grade or better, and solvents were used as received unless otherwise specified. The following reagents were used as received: C_{60} (99.5+%, MER Corp.), *D*-glucosamine hydrochloride (Sigma–Aldrich, MO, USA), DBU (1,8-diaza-bicyclo[5.4.0]undec-7-ene, Sigma–Aldrich), ethyl hydrogen malonate (Sigma–Aldrich), CBr_4 (Sigma–Aldrich), 2-amino-1,3-propanediol (AK Scientific, CA, USA), DIC (*N,N'*-diisopropylcarbodiimide, Sigma–Aldrich) and 1-hydroxybenzotriazole monohydrate (Sigma–Aldrich). The following reagents: Et_3N (Acros), acetic anhydride (Fisher), pyridine (Sigma–Aldrich) and DMF (Sigma–Aldrich) were prepared according to literature procedures by distillation with dehydrating agents and used immediately. Nuclear magnetic resonance spectra were measured on a Bruker 400 MHz NMR Spectrometer with trimethylsilane as an internal standard. The mass spectrometry (MS) spectra for water-insoluble compounds were collected using Autoflex II MALDI-TOF mass spectrometer, and for water-soluble fullerene derivatives – by MS electrospray ionization time-of-flight (ESI-microTOF) mass spectrometer, both instruments from Bruker Daltonics Inc (CA, USA). High-resolution spectra were performed using Shimadzu IT-ToF LC–MS system, and flash chromatography was performed using Agilent 971-FP Flash Purification System. All tested compounds were $\geq 95\%$ pure, as determined by high performance liquid chromatography (HPLC). The purity of all compounds was assessed using a Agilent 1260 equipped with a DAAD detector at 260 nm, RP-column: Eclipse plus C18 (3.5 μm); flow 0.5 ml/min. The time of each measurement was 21 min. Conditions: 0–1.2 min (80% H_2O [0.1% TFA]; 20% acetonitrile); 1.2–8 min [100% acetonitrile]; 8–21 min (80% H_2O [0.1% trifluoroacetic acid]; 20% acetonitrile).

Synthesis of malonate (1) [ethyl 3-oxo-3-(((2*R*,3*R*,4*R*,5*S*,6*R*)-2,4,5-trihydroxy-6-(hydroxymethyl)tetrahydro-2*H*-pyran-3-yl)amino)propanoate]

Ethyl hydrogen malonate (5 mmol) was placed in 250 ml flask, dissolved in 120 ml of anhydrous DMF and cooled to 0°C. Next, DIC (5.5 mmol) was added in three portions during 15 min followed by the addition of glucosamine hydrochloride (5 mmol) and 1-hydroxybenzotriazole monohydrate (5.5 mmol). The reaction mixture was allowed to reach room temperature and was stirred for 18 h in a nitrogen atmosphere. The reaction mixture was then evaporated under reduced pressure, dissolved in 20 ml of methanol and treated with 10 ml of dichloromethane. The resulting white solid was filtered off, and the filtrate was collected and evaporated to obtain yellow oil. The final product was purified from resulting oil after several crystallizations with methanol/DCM as a white solid with 65 % yield.

Synthesis of malonate (2)**[6-(acetoxymethyl)-3-(3-ethoxy-3-oxopropanamido)tetrahydro-2*H*-pyran-2,4,5-triyl triacetate]**

Malonate **1** was dried under lyophilization and suspended in pyridine (100 ml, 1240 mmol) at 0°C, to which acetic anhydride (150 ml, 1590 mmol) was slowly added over the course of 1 h. After reaching 25°C, dissolution occurred and the solution was stirred continuously for 48 h. Methanol (50 ml, 1225 mmol) at 0°C was added to quench the remaining acetic anhydride and the solution was stirred for 1 h. The solvents were removed in vacuo to form yellow oil. The final product was purified using extraction technique (DCM:water) and evaporation of organic phase to form a yellowish gum, which was used without further purification.

Synthesis of C₆₀ monoadduct (3)**[3'-ethoxycarbonyl-3'-(6-(acetoxymethyl)-3-(3-oxopropanamido)tetrahydro-2*H*-pyran-2,4,5-triyl triacetate)-[1,2](C₆₀-1h)[5,6]fullerene]**

C₆₀ (720 mg, 1.00 mmol) was dissolved in freshly distilled toluene (800 ml) with CBr₄ (497 mg, 1.5 mmol) and malonate **2** (461 mg, 1 mmol). At 25°C, 1,8-diazabicyclo[5.4.0]undec-7-ene (DBU, 190 mg, 1.25 mmol) in toluene was added and the reaction was allowed to proceed for 3 h at room temperature under nitrogen atmosphere. Flash chromatography was used (dichloromethane:methanol; 95:5; silica: mallinckrodt, 75–250 µm particles, 150 Å pore size) to isolate the product. Yield: 331.6 mg (33.4%).

Synthesis of C₆₀ (4; hexakis, mixture of regioisomers, also known as Sweet-C₆₀)

Due to higher reactivity of fullerene monoadducts than pristine C₆₀, compound **3** was used as starting material for synthesis of hexakis adducts (mixture of regioisomers). Peracetylated monoadduct **3** (65 mg, 0.055 mmol) was dissolved in freshly distilled toluene (150 ml) with CBr₄ (365 mg, 1.1 mmol) and malonate **2** (254 mg, 0.55 mmol). At 25°C, 1,8-diazabicyclo[5.4.0]undec-7-ene (DBU, 100 mg, 0.66 mmol) in toluene was added slowly over 6 h, and the reaction was allowed to proceed for 36 h at room temperature under nitrogen atmosphere. Flash chromatography was used (gradient from dichloromethane:methanol, 95:5 to 50:50 silica gel:Mallinckrodt, 75–250 µm particles, 150 Å pore size) to isolate the protected product (Supplementary Material [4]). Yield: 74 mg (39 %). Deprotection of acetyl groups was performed in 18 ml of 1,4-dioxane with addition of 2 ml of concentrated hydrochloric acid (36.5 %) and then stirred at room temperature for 5 days. After that time, the final product was purified by dialysis of an aqueous solution of **4** using a cellulose membrane (molecular weight exclusion limit 1.0 kDa; Spectrum Labs, CA, USA) up to the point where electrical conductivity of a purified glycofullerene became equal to the conductivity of distilled water, before being lyophilized.

Dynamic light scattering, -potential analysis & UV–VIS analysis

Dynamic light scattering analysis was performed using a Malvern Nano-ZS90 zetasizer (Malvern Instruments Ltd., Worcestershire, UK) with detection limit ca 1 nm. The Nano-ZS employs noninvasive backscatter optical technology and measures real-time changes in intensity of scattered light. The samples were illuminated by a 633 nm He-Ne laser, and the scattered light was measured at an angle of 173° using a photo-diode. The size distribution of the glycofullerenes was calculated from the particle diffusion coefficient according to the Stokes-Einstein equation. The UV–VIS analysis was performed on a CLARIOstar fluorescent plate reader (BMG LABTECH, NC, USA) across the wavelength range 290–800 nm in 1 nm increments.

Fluorescent labeling of C₆₀ antibody

Fullerene antibody was purchased from Santa Cruz Biotechnology (1-10F-AG) and tagged using Alexa Fluor[®] 647 Antibody Labelling Kit (Molecular Probes). Briefly 1 M solution of sodium bicarbonate was prepared by suspending Component B in 1 ml of deionized water. The antibody concentration was adjusted to concentration 200 ng/ml and dissolved in one-tenth volume of the 1 M sodium bicarbonate from the previous step. Next 500 µl of buffered antibody was added to the vial of Alexa Fluor[®] dye, inverted to mix and incubated for 90 min at room temperature. The fluorescent antibody was purified using special purification column by loading reaction mixture to the column and centrifuging the column at 1100 x g for 5 min followed by collecting the labeled antibody.

Cell culture

Human PDAC line PANC-1 was obtained from American Type Culture Collection (ATCC, VA, USA). The PANC-1 cells were maintained in DMEM (Thermo Fischer Scientific, MA, USA) with 10% fetal bovine serum (FBS, Sigma, NY, USA). A total of 2% penicillin–streptomycin solution (Sigma) was added to the media of all PDAC lines. Human PSCs were provided by Hwang *et al.* (UT-MD Anderson Cancer Center, TX, USA). Fresh tissue was obtained from residual PDAC specimens from patients undergoing primary surgical resection at The University of Texas M.D. Anderson Cancer Center. All human samples were obtained in accordance with the policies and practices of the Institutional Review Board of The University of Texas M.D. Anderson Cancer Center. The PSCs were isolated and prepared as previously described [32]. Briefly, PSCs were prepared by the outgrowth method [37]. Fresh tissue was obtained from residual PDAC specimens from patients undergoing primary surgical resection at The University of Texas M.D. Anderson Cancer Center. Tumor samples were minced and seeded in six-well plates containing 15% FCS/DMEM, L-glutamine (2 mmol/l), penicillin/streptomycin and amphotericin. A total of 5 days later, cells were able to grow out from the tissue clumps. When PSCs grew to confluence, cells were trypsinized and passaged at a 1:3 ratio. Cell purity was determined by immunohistochemistry for α-SMA, vimentin and desmin, as well as morphology (spindle-shaped cells with cytoplasmic extensions) and positive staining with Oil Red O (lipid inclusions were visualized). Furthermore, PSC derived from the pancreatic tumor of a patient, who had received no prior therapy before surgery, were immortalized using lentiviral vector with human telomerase (hTERT) or SV40 large T antigen (TAg) through plasmids containing TAg (pHIV7-CNPO-TAg) and hTERT (pHIV7-CNPO-hTERT) as previously described in detail [38]. The PSCs carrying the hTERT or SV40-T were selected in 1–3 mg/ml G418 for 3 weeks (Invitrogen). Cells were maintained in DMEM with 10% FBS at 37°C in a humidified atmosphere of 5% CO₂.

Cellular localization of Sweet-C₆₀ using confocal microscopy

Particle localization studies were performed using PSC cells cultured as previously described [39]. Fullerene staining involved a previously developed fullerene antibody being used (1-10F-A8; Santa Cruz Biotechnology). The antibody was tagged with Alex Fluor[®] 647 dye as described above. For localization studies 3×10^5 cells were seeded onto round 3 mm diameter #1.5 coverslips (Ted Pella, Inc., CA, USA) placed in the bottom of a 12-well plate. Cells were allowed to adhere for 3 h prior to particle exposure. After adherence, cells were supplemented with media containing a range of Sweet-C₆₀ concentrations: 0, 0.01, 0.1 and 1 mg/ml. Cells were then incubated for either 3 or 24 h prior to being prepped for confocal microscopy. After exposure, the media was removed and the coverslips were thoroughly washed with phosphate-buffered saline (PBS) to remove any residual particles. Cells were then stained using the Cytopainter Lysosome/Mitochondria/Nuclear staining Reagent (Abcam) per manufacturer's instructions. After rinsing, cells underwent the following optimized steps; fixation in 4% PFA for 15 min followed by rinsing with PBS; permeabilization in 0.1% Triton X for 5 min followed by PBS rinse; block and permeabilization in 5% FBS + 0.1% Triton X for 15 min, and fullerene antibody staining which was added directly to the block/perm solution at a final volume concentration of 1:300 and allowed to stain for 30 min at room temperature protected from light. The coverslips were then thoroughly rinsed prior to mounting onto slides, using Prolong Gold Antifade mountant (ThermoFisher). Slides were left for 48 h to allow the Prolong Gold Antifade mountant to dry. Images were captured using Nikon AIRMP Multiphoton Confocal Microscope. Laser power, gain and LUTs were set standard across all images. Co-localization was determined by segmenting the whole cell, the cytoplasm only and the nuclei regions. The PFA was then calculated using [equation 1](#) (where ID depicts the integrated density of the region of interest, A is area of region of interest and M is the mean background fluorescence). Mean background fluorescence was calculated by measuring the mean intensity of pixels when a region containing no cells was selected.

Image analysis was carried out using ImageJ software (NIC, MD, USA)

$$\text{CTCF} = \text{ID} - (\text{A} \times \text{M}) \quad (\text{Equation 1})$$

Cytotoxicity studies using flow cytometry

Sweet-C₆₀ cytotoxicity studies were performed in PANC1 and PSC cell lines (ATCC). Cells were plated in 12-well plates at 3×10^5 cells per well and allowed to adhere for 24 h prior to particle exposure. Once adhered the media was removed and cells washed twice with PBS. Samples of Sweet-C₆₀ were dissolved in DMEM media at a 10 mg/ml concentration and vortexed well to ensure a monodispersed particle stock. Sweet fullerenes were then added to each well to achieve total well particle concentrations of 0, 0.01, 0.1 or 1 mg/ml. Cells were then incubated for either 3 or 24 h prior to being analyzed for cytotoxicity. After the required exposure time cells were collected via trypsinization and rinsed once with Annexin binding buffer prior to staining. Cells were then stained with the Dead Cell Apoptosis Kit with Annexin V-FITC and PI for flow cytometry (ThermoFisher) per the manufacturer's instructions. Cells were analyzed using a LSRII flow cytometer (BD Biosciences, CA, USA) and cellular percentages were recorded as live cells (annexin-, PI-), early apoptotic (annexin+, PI-), late apoptotic (annexin+, PI+) or dead (annexin-, PI+). Appropriate biologic and single stain controls were used to set each gate. Each experiment included triplicate biologic repeats.

Anticancer Sweet-C₆₀ photodynamic therapy

Cytotoxicity was quantified using DNA-binding DRAQ7 (Biostatus Ltd, UK) staining, which is a far-red fluorescent dye. The PDAC cells were seeded at a concentration of 5000 cells per well in Greiner Bio One Cellstar[®] tissue culture 96-well plate for 24 h. Once adhered to the plate bottom, the cells were washed with PBS and then incubated with 0.1 mg/ml concentration of Sweet-C₆₀ was mixed in media for 24 h. Any residual Sweet-C₆₀ was then washed off the cells by rinsing the cells three-times with PBS. For PDT therapy, 150 µl of PBS was added to the plate before it being placed on the PDT unit for 30 min for treatment either with blue LED (450 nm) or green LED (520 nm) light. After the PDT treatment had finished, the PBS was gently replaced with fresh DMEM media containing 3 µM concentration of DRAQ7 (Biostatus Ltd, UK). For ambient light control plates the same procedures were followed; however, the LED unit was not switched on. Positive kill control plates were placed in a microwave at high power for 20 s to induce 100% cell death that was verified using microscopy. Cells were imaged at 10x magnification in two channels: the DRAQ7 (Cy5, Absorbance 600 nm emission 697 nm) and the bright-field. Cell death was quantified by the measure of the DRAQ7 signals at the 3-h and the 24-h time points using ImageJ analysis software (NIH). Each treatment group was performed in triplicate and the segmentation algorithm used to count the DRAQ7 signal was verified via a manual count of signals in the first plate of each group (more detail in next section). The temperature in the center well containing media of a 96-well plate was measured via temperature probes and an IR camera during the course of the 30-min treatment time to rule out any effect being due to hyperthermia.

Statistical analysis

All data are represented as mean with error bars representing standard deviation. For co-localization studies comparisons were made between either whole cell or nucleus cell total fluorescence analysis for all concentrations using an ANOVA and multiple comparison test with Bonferroni's correction. For other studies Student's *t*-test was performed. For other experiments, differences between groups were assessed using the Student's *t*-test.

Results

An overview of the Sweet-C₆₀ chemical synthetic pathway is shown in Figure 1. A detailed description of each intermediate can be found in the Supplementary Information. We optimized and applied nucleophilic cyclopropanation reactions (Bingel reactions) as an efficient method for obtaining the C₆₀ sugar derivatives in moderate yields. Acetate protecting groups were used to block all glucosamine hydroxyl groups during the cyclopropanation reactions. The best deprotection results were obtained when a 1M HCl solution in 1,4-dioxane was used. This method was especially attractive over common methods of long and laborious dialysis using K₂CO₃. The ¹H and ¹³C-NMR studies (Supplementary Information) have shown that the α-isomer of malonic glucosamide is formed preferentially (signals at 5.12 ppm and 90 ppm, respectively). Unfortunately, the symmetrical glucosamine derivative of malonic acid was not synthesized, probably due to a steric hindrance problem for symmetrical malonate.

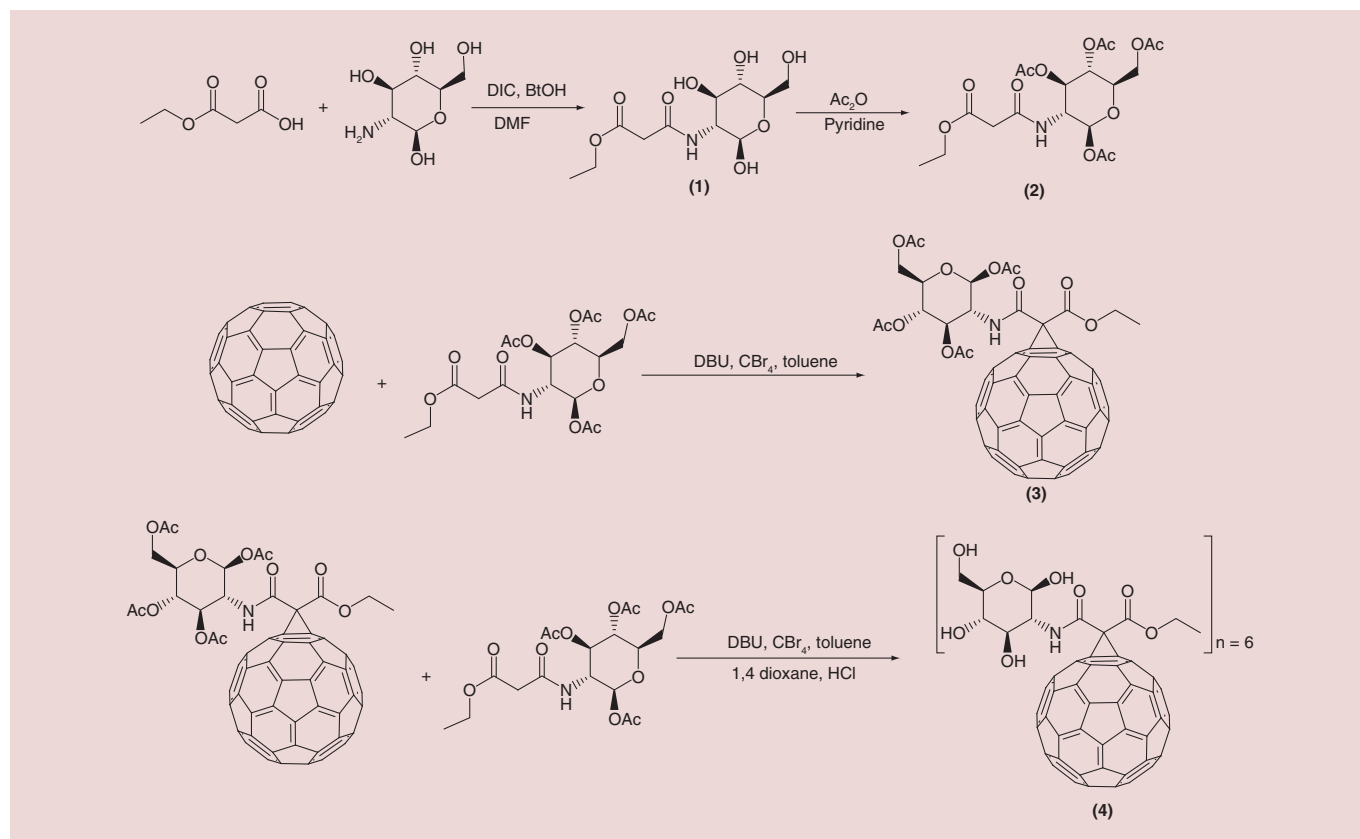


Figure 1. Scheme depicting the synthesis of Sweet-C₆₀.

To prepare the C₆₀ monoadduct of the malonoamide **2**, the method of *in situ* generation of the active brominated intermediate (with CBr₄ and DBU) was carried out. The reaction, as shown in **Figure 1**, was found to proceed nicely at room temperature within 3 h. The MALDI-TOF MS data of malonates **1** and **2** are found in Supplementary **Figure 1** and **2**, respectively. Time control is crucial at this step due to fast formation of bisadducts. A molecular ion peak at 1177.9 Da (Supplementary **Figure 3**) was observed in the MALDI-TOF MS (calculated for C₇₉H₂₅NO₁₂, 1179.14 Da) as well as a single spot observed by thin layer chromatography. Moreover, the structure of monoadduct **3** was confirmed by ¹H and ¹³C nuclear magnetic resonance (NMR) spectroscopy, showing high symmetry in the carbon spectrum (Supporting Information). The C₆₀ hexakis-adducts were obtained by the second Bingel reaction from monoadduct **3** as the starting material, due to its higher reactivity. The most efficient procedure was accomplished when the ratio between C₆₀, malonate, DBU and CBr₄ was 1:10:10:20 and the DBU was added in six portions over 6 h. The MALDI TOF MS spectra of the acetyl protected fullerenes are shown in Supplementary **Figure 4**. A molecular ion peak from deprotected sodium adduct of **4** (i.e., Sweet-C₆₀) was obtained at 2489.9 Da with a small signal of pentakis isomer at 2198.3 Da (Supplementary **Figure 5**).

It has been previously reported in the literature that water-soluble C₆₀ derivatives (i.e., C₆₀-serinol, a.k.a. C₆₀-ser) tend to form aggregates in aqueous solutions [13]. These aggregates are in dynamic equilibrium, forming smaller and larger forms, which can be detected using dynamic light scattering or scanning electron microscopy and can be easily destroyed by the addition of organic solvent or changing the ionic strength of the medium by addition of salts [40,41]. Interestingly, our recent observations indicate that these dynamic C₆₀-ser aggregates are built up of a single layer of C₆₀-ser molecules, with water molecules locked inside a hollow core structure [13]. As can be seen in Supplementary **Figure 6A**, the Sweet-C₆₀ seems to predominantly aggregate at around 150 nm with no smaller subset aggregates. potential measurements (Supplementary **Figure 6B**) also indicate a surface of charge of -27 mV, indicating a relatively good degree of stability. Given the potential of Sweet-C₆₀ to exhibit PDT behavior, an optical absorption assessment was also obtained using UV-VIS spectroscopy. As can be seen in Supplementary **Figure 7**, Sweet-C₆₀ tends to absorb better in the blue region of the spectrum (i.e., <450 nm).

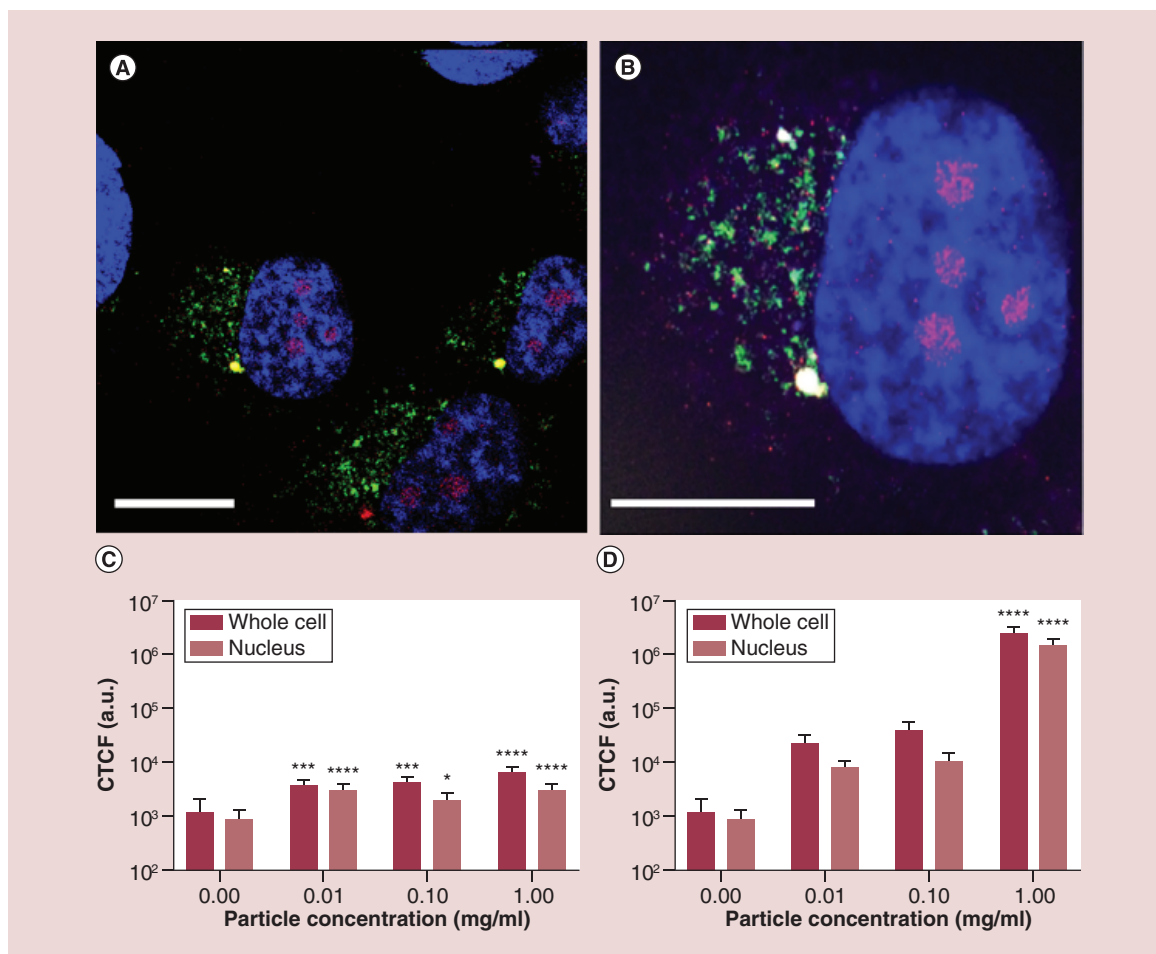


Figure 2. Co-localization of Sweet-C₆₀ (1 mg/ml) in pancreatic stellate cells. (A & B) Confocal micrograph depicting pancreatic stellate cells blue regions, 4',6-diamidino-2-phenylindole (DAPI) represents stained nucleus, green regions fluorescein isothiocyanate represents mitochondrial staining, red regions tetramethylrhodamine represents lysosomes and magenta represents antibody-glycofullerene conjugate (ALEXAFLUOR 647), white bar represents 50 μm). (C) The corrected total cell fluorescence signal localization of fluorescently labeled antibody–Sweet-C₆₀ conjugate in pancreatic stellate cells for 3 h and (D) 24 h. Data are represented as mean with error bars representing standard deviation.

Discussion

We have previously documented cellular internalization of PromoFluor-633-conjugated malonodiserinolamide-derivatized [60]fullerene (C₆₀-serPF), followed by its cellular distribution using confocal microscopy [12]. We demonstrated that water-soluble, nonionic C₆₀serPF can localize to the nucleus and permeate into a wide variety of tissues, including malignant liver tumors and brain. Moreover, recent studies have shown that C₆₀serPF extravasates more into orthotopic breast tumor tissue than into contralateral mammary fat pad, which could be modulated by RF hyperthermia [14].

In the present study, we focused our attention on visualizing nonfluorescent, Sweet-C₆₀. To achieve this goal, we fluorescently labeled a mouse monoclonal antibody specific for fullerenes (1-10F-A8; Santa Cruz Biotechnology) with Alexa Fluor[®] 647 dye, following the recently developed procedure of Miao *et al.*, whereby a selected antibody was raised against a C₆₀ fullerene derivative conjugated to thyroglobulin and used for the detection of nanoC₆₀ [39]. Due to the possibility of nonspecific staining occurring from fluorescence at 0 μM Sweet-C₆₀ concentration, we validated the significance of our results by investigating the relationship between a range of Sweet-C₆₀ concentrations after incubation with cells and the resulting fluorescence signal (data not shown). Figure 2 indicated that Sweet-C₆₀ localizes preferentially in the nucleus of PSC cells, with some localization in the cell cytoplasm. These results are in accordance with our previous findings, showing that water-soluble C₆₀serPF also localizes within the cell

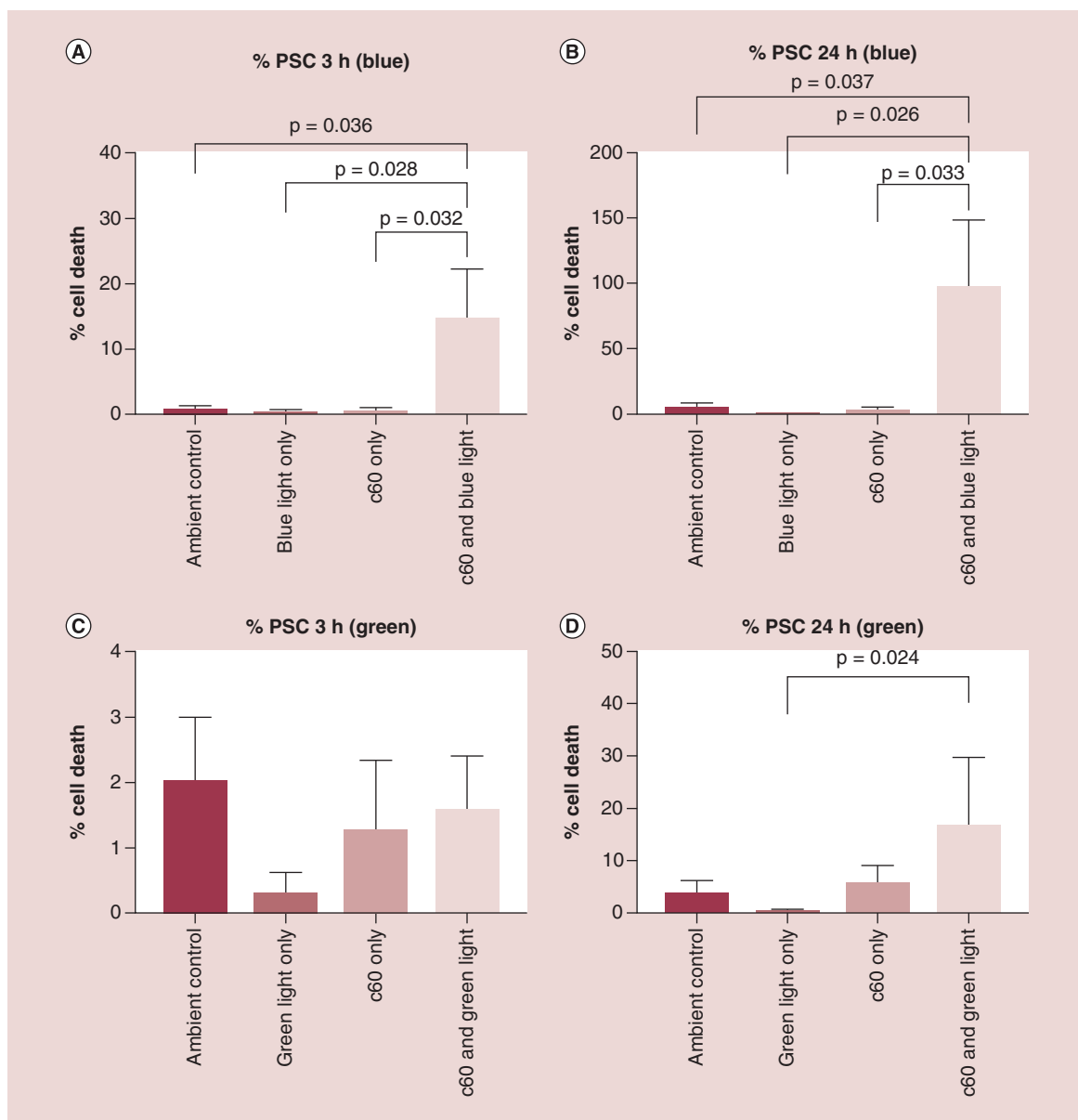


Figure 3. Phototoxicity effects of Sweet-C₆₀ (0.1 mg/ml) on pancreatic stellate cells. (A) Number of dead pancreatic stellate cells at 3 h and (B) 24 h time point, after blue and light exposure. (C) Number of dead pancreatic stellate cells at 3 h and (D) 24 h time point, after green light exposure.

nucleus [12]. A comparison of cell fluorescence signals with different fullerene concentrations shows an enhanced and overwhelming signal that predominantly originates within the cell nucleus.

In order to quantify the proportion of fluorescence signals registered for the whole cell and also only for nuclei, cell total fluorescence analysis was conducted. As shown in Figure 2C and D after 3 h of incubation, only a small increase of fluorescence signal from cell area in comparison from the negative control (0 mg/ml) can be seen. This can be related to the slow uptake of Sweet-C₆₀ into the cells. On the other hand, when cells are treated with Sweet-C₆₀ for a longer period of time (24 h) and in high concentration (1 mg/ml), the difference between incubated cells and control cells was four orders of magnitude. The comparison of distribution of fluoresce signal inside the cell area indicated predominant localization of Sweet-C₆₀ into the cell nuclei. A weak fluorescence signal is also present in the cytoplasm regions, which is however, most likely due to statistical and biotransport variation.

The cytotoxicity effects of water-soluble fullerene derivatives have been studied extensively during the last 10 years, mainly due to their implication and impact in various nanotherapeutics (as previously discussed).

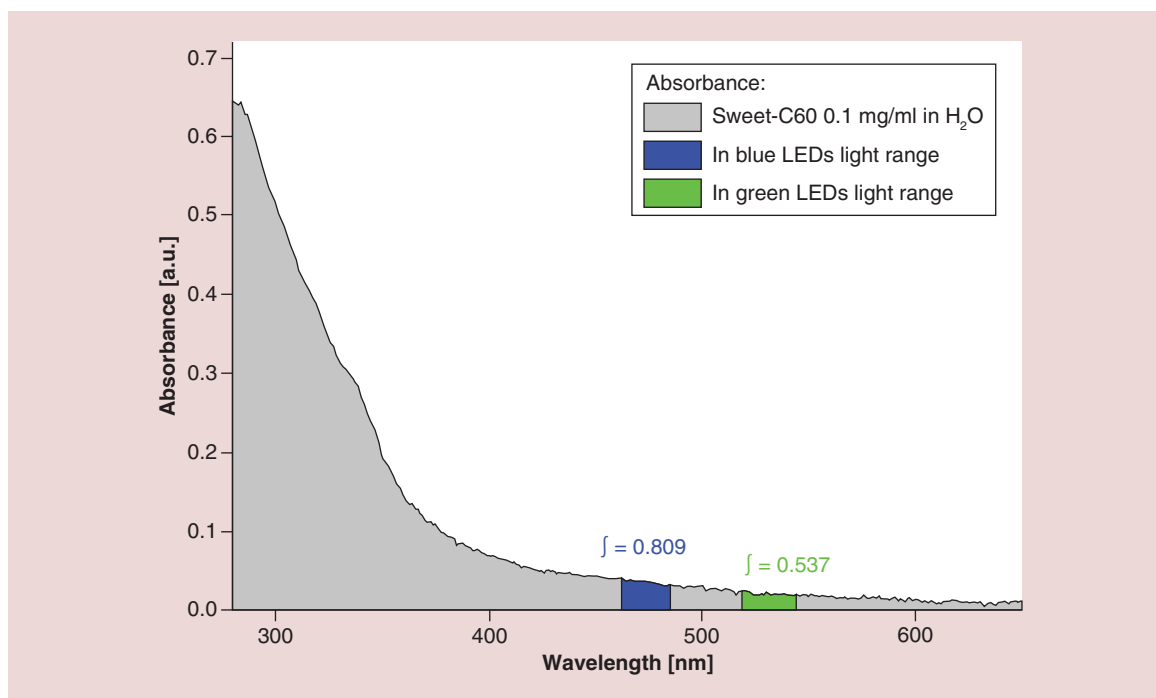


Figure 4. The integral of Sweet-C₆₀ absorbance in blue and green light region.

Others and ourselves have previously demonstrated that water-soluble fullerenes exhibit negligible toxicity [12,42]. Interestingly, some recent studies have shown cytoprotective effects of fullerenes, acting as scavengers of reactive oxygen species (ROS), especially for gadofullerenes and C₆₀(OH)₂₄ nanomaterials [43,44]. Furthermore, a few possible mechanisms of action have been proposed to play crucial roles in observed cytotoxic effects, which include ROS generation, solvent contamination (during fabrication, i.e., tetrahydrofuran impurities) and autophagy-mediated cell death [42,45,46]. We investigated the concentration dependent cytotoxicity profile of the Sweet-C₆₀ across the range 0.01–1 mg/ml in both PSC and PANC-1 cells using cell flow cytometry with markers for cellular apoptosis (Annexin V-FITC) and viability (propidium iodide, PI). As is shown in Supplementary Figure 8, negligible toxicity was seen across all concentrations. In addition, 1.0 mg/ml was chosen as the working concentration for our cell internalization studies to coincide with our previous internalization studies on C₆₀serPF [12].

In general, fullerenes exhibit good photostability and efficiency to photogenerated singlet oxygen and free radicals. The absorption of visible light combined with efficient intersystem crossing to long-lived triplet states allows fullerenes to generate various types of ROS after illumination [47]. For example, in polar solvents, illuminated fullerene derivatives generate reduced oxygen forms such as the superoxide radical (O₂⁻) and hydroxyl radical (·OH). In contrast, in nonpolar solvents, when solutions of C₆₀ are exposed to light of certain wavelengths, mainly singlet oxygen (¹O₂) are generated [47]. This physical phenomenon of fullerene derivatives has a practical application, whereby C₆₀ derivatives are therapeutically used via photodynamic or photocatalytic pathways [48,49].

Here, we investigated whether Sweet-C₆₀ can have a cytotoxic effect upon PSCs when illuminated with LED blue and green light (emission spectra Supplementary Figure 9), the cytotoxic mechanism of which is hypothesized to be from ROS generation. The phototoxicity studies presented in Figure 3 exhibit a strong photodynamic cytotoxic effect for PSCs after blue (E_m 470 nm) and green (E_m 530 nm) LED treatment. A similar but slight reduced effect was also observed for PANC-1 cells (Supplementary Figure 10). This could be due PANC-1 cells having elevated heat shock protein and enzymes to deal with ROS (e.g., due to different redox potentials in tumors and cancer cells). The fast cytotoxicity observed at 3 h (Figure 3), especially after blue light illumination, suggests that necrotic action is occurring. The increase in toxicity exhibited at 24 h suggests a delayed, programmed cell death mechanism at play, for example, apoptosis. The integral of Sweet-C₆₀ absorbance in blue light region is 0.809, whereas in the green spectrum region is 0.537 (a.u.). This leads to the conclusion that during green light illumination Sweet-C₆₀ can be excited 33% less effectively than after the blue light (Figure 4). Moreover, the generation of the excited form

Summary points

- Glucosamine-based and highly water-soluble Sweet-C₆₀ has been synthesized in moderate yields using a Bingel–Hirsch approach.
- The C₆₀ derivative shows negligible *in vitro* toxicity even at high doses (1 mg/ml).
- [60]fullerene derivative localizes preferentially in the nucleus of pancreatic stellate cells, with some localization in the cell cytoplasm.
- Synthesized Sweet-C₆₀ is phototoxic when illuminated with blue or green LED system, and could be used in combinatorial therapies in which cytostatic agents will be covalently conjugated to the Sweet-C₆₀ scaffold.

of Sweet-C₆₀ is dependent not only on the quantity of photons (as compared above) but also to the photons energy. Blue light is more effective in that process, but the effective depth of optical penetration is smaller compared with green light. However, in regards to *in vitro* studies using monolayers of cells, the light penetration and diffraction should not be a crucial factor. The difference in biological response to photodynamic effect in PSCs and PANC-1 cells is most likely explained by smaller photon absorption efficiency of green light compared with blue light. Apparently, according to absorbance spectrum (Figure 4), both light types are able to excite Sweet-C₆₀ molecule effectively enough to generate ROS cascade and induce cell death. In conclusion, the postulated different cell death mechanisms indicate, that major ROS amount after blue light illumination leads to membrane destruction and cells lesions in a short time scale (green light will indicate minor ROS amount/types and create the time window for cells to repair and/or program cell death).

Conclusion

The PSCs are a subset of cells involved with the establishment of dense stroma regions in cases of advanced pancreatic adenocarcinoma. As such, new methods to target and treat PSCs are needed. Our results show predominant cellular nuclear internalization of the hexakis-glucosamine C₆₀ derivative (Sweet-C₆₀). In addition, the Sweet-C₆₀ is inherently nontoxic up to concentrations of 1 mg/ml, and displays strong photodynamic cytotoxic behavior, when illuminated with both blue and green light. This phototoxic behavior was also observed for pancreatic cancer cells (PANC-1).

Future perspective

Traditional gemcitabine-based chemotherapy of pancreatic cancer rarely results in cure; therefore, nanotherapeutic approaches should be further studied. In particular, more studies should be focused on patient-derived primary PSC and their uptake of Sweet-C₆₀. Furthermore, the level of GLUT-1 protein should be measured in PSC cell lines using western blot and PCR techniques and extended to analysis of GLUT inhibitors and their influence on Sweet-C₆₀ uptake. Presented photodynamic effect of glycofullerenes should be also investigated in 3D-spheroid models for better understanding LED penetration and stroma effects. The ROS generation measurements such as detection of singlet oxygen and superoxide radicals using flash photolysis and EPR-spin trapping would also be a good addition for those studies.

Supplementary data

To view the supplementary data that accompany this paper please visit the journal website at: www.futuremedicine.com/doi/full/10.2217/nnm-2018-0239

Acknowledgments

Our thanks are extended to R Hwang of the Department of Surgical Oncology, University of Texas MD Anderson Cancer who kindly provided the pancreatic stellate cells.

Financial & competing interests disclosure

M Serda, JM Newton, MJ Ware, S Sachdeva, M Krzykawska-Serda, J Law, L Nguyen, SA Curley and SJ Corr acknowledge the funding of Kanzius Foundation and NIH U54CA143837. LJ Wilson also thanks the Welch Foundation (grant number C-0627) for support. Additionally, M Serda thanks National Science Center (Poland) for the support (grant number UMO-2016/23/D/NZ7/00912). MJ Ware and SJ Corr acknowledge the support of St Luke's Foundation Philip Salem Award. JM Newton acknowledges financial support from the NIGMS T32 predoctoral training (grant number T32GM088129) and NIDCR F31 NRSA training grant (grant

number F31DE026682) both of the NIH. This project was supported by the Cytometry and Cell Sorting Core at Baylor College of Medicine with funding from the NIH (grant numbers NIAID P30AI036211, NCI P30CA125123 and NCRR S10RR024574) and the assistance of JM Sederstrom. This content is solely the responsibility of the authors and does not necessarily represent the official views of the NIH. The authors declare no conflicts of interest.

The authors have no other relevant affiliations or financial involvement with any organization or entity with a financial interest in or financial conflict with the subject matter or materials discussed in the manuscript apart from those disclosed.

No writing assistance was utilized in the production of this manuscript.

Ethical disclosure

The authors state that they have obtained appropriate institutional review board approval or have followed the principles outlined in the Declaration of Helsinki for all human or animal experimental investigations. In addition, for investigations involving human subjects, informed consent has been obtained from the participants involved.

Author contributions

Conception and design: M Serda, MJ Ware, M Krzykawska-Serda, LJ Wilson, SJ Corr and SA Curley. Acquisition of data: M Serda, MJ Ware, M Krzykawska-Serda, JM Newton, S Sachdeva. Analysis and interpretation of the data: M Serda, MJ Ware, M Krzykawska-Serda, JM Newton, S Sachdeva, and SJ Corr. Manuscript preparation: M Serda, SJ Corr, MJ Ware, JM Newton and M Krzykawska-Serda wrote the manuscript. All authors read and approved the final manuscript.

Blinded for review

Methods and materials:

Cell culture: R. Hwang (UT-MD Anderson Cancer Center, Houston TX); The University of Texas M.D. Anderson Cancer Center; The Institutional Review Board of The University of Texas M.D. Anderson Cancer Center; The University of Texas M.D. Anderson Cancer Center.

References

Papers of special note have been highlighted as: ● of interest; ●● of considerable interest

1. Kroto HW, Heath JR, O'Brien SC, Curl RF, Smalley RE. C₆₀: buckminsterfullerene. *Nature* 318, 162 (1985).
2. Acquah SFA, Penkova AV, Markelov DA, Semisalov AS, Leonhardt BE, Magi JM. Review – the beautiful molecule: 30 years of C₆₀ and its derivatives. *ECS J. Solid State Sci. Technol.* 6(6), M3155–M3162 (2017).
3. Thakral S, Thakral NK. Potential medical applications of fullerenes: an overview. In: *Bio-Nanotechnology*. Blackwell Publishing Ltd., Fereidoon Shahidi, Newfoundland, Canada, 424–441 (2013).
4. Mroz P, Tegos GP, Gali H, Wharton T, Sarna T, Hamblin MR. Photodynamic therapy with fullerenes. *Photochem. Photobiol. Sci.* 6(11), 1139–1149 (2007).
- **Review of photodynamic therapy using water-soluble fullerenes.**
5. Mroz P, Pawlak A, Satti M *et al.* Functionalized fullerenes mediate photodynamic killing of cancer cells: Type I versus Type II photochemical mechanism. *Free Radic. Biol. Med.* 43(5), 711–719 (2007).
6. Bolskar RD. Fullerenes for drug delivery. In: *Encyclopedia of Nanotechnology*. Bhushan B (Ed.). Springer, The Netherlands, Dordrecht, 1267–1281 (2016).
7. Sitharaman B, Zakharian TY, Saraf A *et al.* Water-soluble fullerene (C(60)) derivatives as nonviral gene-delivery vectors. *Mol. Pharm.* 5(4), 567–578 (2008).
8. Bolskar RD. Gadolinium endohedral metallofullerene-based MRI contrast agents. In: *Medicinal Chemistry and Pharmacological Potential of Fullerenes and Carbon Nanotubes*. Cataldo F, Da Ros T (Eds.). Springer, The Netherlands, Dordrecht, 157–180 (2008).
9. Tegos GP, Demidova TN, Arcila-Lopez D *et al.* Cationic fullerenes are effective and selective antimicrobial photosensitizers. *Chem. Biol.* 12(10), 1127–1135 (2005).
10. Gharbi N, Pressac M, Hadchouel M, Szwarc H, Wilson SR, Moussa F. [60]Fullerene is a powerful antioxidant *in vivo* with no acute or subacute toxicity. *Nano Lett.* 5(12), 2578–2585 (2005).
11. Zakharian TY, Seryshev A, Sitharaman B, Gilbert BE, Knight V, Wilson LJ. A fullerene–paclitaxel chemotherapeutic: synthesis, characterization, and study of biological activity in tissue culture. *J. Am. Chem. Soc.* 127(36), 12508–12509 (2005).
- **The first report on covalent conjugation of C₆₀ with paclitaxel.**
12. Raouf M, Mackeyev Y, Cheney MA, Wilson LJ, Curley SA. Internalization of C₆₀ fullerenes into cancer cells with accumulation in the nucleus via the nuclear pore complex. *Biomaterials* 33(10), 2952–2960 (2012).
- **The first report describing studies on biodistribution of fluorescently labeled C₆₀ in cancer cells.**

13. Lapin NA, Vergara LA, Mackeyev Y *et al.* Biotransport kinetics and intratumoral biodistribution of malonodiserinamide-derivatized [60]fullerene in a murine model of breast adenocarcinoma. *Int. J. Nanomed.* 12, 8289–8307 (2017).
14. Lapin NA, Krzykawska-Serda M, Dilliard S *et al.* The effects of non-invasive radiofrequency electric field hyperthermia on biotransport and biodistribution of fluorescent [60]fullerene derivative in a murine orthotopic model of breast adenocarcinoma. *J. Control. Rel.* 260, 92–99 (2017).
- **Paper describing biodistribution of C₆₀-serPF in the living mouse using intravital microscopy.**
15. Lara NC, Haider AA, Wilson LJ, Curley SA, Corr SJ. Unique heating curves generated by radiofrequency electric-field interactions with semi-aqueous solutions. *Appl. Phys. Lett.* 110(1), 013701 (2017).
16. Lara NC, Haider AA, Ho JC *et al.* Water-structuring molecules and nanomaterials enhance radiofrequency heating in biologically relevant solutions. *Chem. Commun.* 52(85), 12630–12633 (2016).
17. Éva Tóth RDB, Borel A, González G *et al.* Water-soluble gadofullerenes: toward high-relaxivity, pH-responsive MRI contrast agents. *J. Am. Chem. Soc.* 127(2), 799–805 (2005).
18. Hartman KB, Wilson LJ. Carbon nanostructures as a new high-performance platform for MR molecular imaging. In: *Bio-Applications of Nanoparticles*. Chan WCW (Ed.) Springer, NY, USA, 74–84 (2007).
19. Sitharaman B, Tran LA, Pham QP *et al.* Gadofullerenes as nanoscale magnetic labels for cellular MRI. *Contrast Media Mol. Imaging* 2(3), 139–146 (2007).
20. Fejes Z, Hadházi Á, Rűth E *et al.* Synthesis of ether-linked [60]fullerene glycoconjugates by nucleophilic cyclopropanation. *Chem. Paper* 69(6), 896–900 (2015).
21. Isobe H, Mashima H, Yorimitsu H, Nakamura E. Synthesis of fullerene glycoconjugates through sulfide connection in aqueous media. *Org. Lett.* 5(23), 4461–4463 (2003).
22. Kato H, Böttcher C, Hirsch A. Sugar balls: synthesis and supramolecular assembly of [60]fullerene glycoconjugates. *Eur. J. Org. Chem.* 2007(16), 2659–2666 (2007).
23. Currie CJ, Poole CD, Gale EAM. The influence of glucose-lowering therapies on cancer risk in Type 2 diabetes. *Diabetologia* 52(9), 1766–1777 (2009).
24. Elstrom RL, Bauer DE, Buzzai M *et al.* Akt stimulates aerobic glycolysis in cancer cells. *Cancer Res.* 64(11), 3892 (2004).
25. Ito H, Duxbury M, Zinner MJ, Ashley SW, Whang EE. Glucose transporter-1 gene expression is associated with pancreatic cancer invasiveness and MMP-2 activity. *Surgery* 136(3), 548–556 (2004).
26. Reske SN, Grillenberger KG, Glatting G *et al.* Overexpression of glucose transporter 1 and increased FDG uptake in pancreatic carcinoma. *J. Nucl. Med.* 38(9), 1344–1348 (1997).
27. Shimizu T, Okamoto I, Tamura K *et al.* Phase I clinical and pharmacokinetic study of the glucose-conjugated cytotoxic agent d-19575 (glufosfamide) in patients with solid tumors. *Cancer Chemother. Pharmacol.* 65(2), 243 (2009).
28. Basturk O, Singh R, Kaygusuz E *et al.* GLUT-1 expression in pancreatic neoplasia: implications in pathogenesis, diagnosis, and prognosis. *Pancreas* 40(2), 187–192 (2011).
29. Apte MV, Park S, Phillips PA *et al.* Desmoplastic reaction in pancreatic cancer: role of pancreatic stellate cells. *Pancreas* 29(3) 179–187 (2004).
30. Ware MJ, Keshishian V, Law JJ *et al.* Generation of an *in vitro* 3D PDAC stroma rich spheroid model. *Biomaterials* 108, 129–142 (2016).
31. Ene-Obong A, Clear AJ, Watt J *et al.* Activated pancreatic stellate cells sequester CD8(+) T-cells to reduce their infiltration of the juxtatumoral compartment of pancreatic ductal adenocarcinoma. *Gastroenterology* 145(5), 1121–1132 (2013).
32. Hwang RF, Moore T, Arumugam T *et al.* Cancer-associated stromal fibroblasts promote pancreatic tumor progression. *Cancer Res.* 68(3), 918–926 (2008).
33. Tang D, Yuan Z, Xue X *et al.* High expression of galectin-1 in pancreatic stellate cells plays a role in the development and maintenance of an immunosuppressive microenvironment in pancreatic cancer. *Int. J. Cancer* 130(10), 2337–2348 (2012).
34. Wilson JS, Pirola RC, Apte MV. Stars and stripes in pancreatic cancer: role of stellate cells and stroma in cancer progression. *Front. Physiol.* 5, 52 (2014).
35. Xu Z, Vonlaufen A, Phillips PA *et al.* Role of pancreatic stellate cells in pancreatic cancer metastasis. *Am. J. Pathol.* 177(5), 2585–2596 (2010).
36. Olive KP, Jacobetz MA, Davidson CJ *et al.* Inhibition of hedgehog signaling enhances delivery of chemotherapy in a mouse model of pancreatic cancer. *Science* 324(5933), 1457–1461 (2009).
37. Bachem MG, Schunemann M, Ramadani M *et al.* Pancreatic carcinoma cells induce fibrosis by stimulating proliferation and matrix synthesis of stellate cells. *Gastroenterology* 128(4), 907–921 (2005).
38. Erkan M, Kleeff J, Reiser C *et al.* Preoperative acute pancreatitis in periampullary tumors: implications for surgical management. *Digestion* 75(2–3), 165–171 (2007).
39. Miao Y, Xu J, Shen Y *et al.* Nanoparticle as Signaling protein mimic: robust structural and functional modulation of CaMKII upon specific binding to fullerene C₆₀ nanocrystals. *ACS Nano* 8(6), 6131–6144 (2014).

40. Brant J, Lecoanet H, Wiesner MR. Aggregation and deposition characteristics of fullerene nanoparticles in aqueous systems. *J. Nanopart. Res.* 7(4), 545–553 (2005).
41. Laus S, Sitharaman B, Tóth É *et al.* Destroying gadofullerene aggregates by salt addition in aqueous solution of Gd@C(60)(OH)(x) and Gd@C(60)[C(COOH(2))](10). *J. Am. Chem. Soc.* 127(26), 9368–9369 (2005).
42. Sayes CM, Fortner JD, Guo W *et al.* The differential cytotoxicity of water-soluble fullerenes. *Nano Lett.* 4(10), 1881–1887 (2004).
43. Xiao L, Takada H, Gan Xh, Miwa N. The water-soluble fullerene derivative ‘Radical Sponge[®]’ exerts cytoprotective action against UVA irradiation but not visible-light-catalyzed cytotoxicity in human skin keratinocytes. *Bioorg. Med. Chem. Lett.* 16(6), 1590–1595 (2006).
44. Yin J-J, Lao F, Fu PP *et al.* The scavenging of reactive oxygen species and the potential for cell protection by functionalized fullerene materials. *Biomaterials* 30(4), 611–621 (2009).
45. Zhang Q, Yang W, Man N *et al.* Autophagy-mediated chemosensitization in cancer cells by fullerene C₆₀ nanocrystal. *Autophagy* 5(8), 1107–1117 (2009).
- **The fullerene nanocrystals can resensitize cancer cells by autophagy-mediated mechanism.**
46. Isakovic A, Markovic Z, Todorovic-Markovic B *et al.* Distinct cytotoxic mechanisms of pristine versus hydroxylated fullerene. *Toxicol. Sci.* 91(1), 173–183 (2006).
47. Mroz P, Pawlak A, Satti M *et al.* Functionalized fullerenes mediate photodynamic killing of cancer cells: Type I versus Type II photochemical mechanism. *Free Radic. Biol. Med.* 43(5), 711–719 (2007).
48. Sharma SK, Chiang LY, Hamblin MR. Photodynamic therapy with fullerenes *in vivo*: reality or a dream? *Nanomedicine (Lond.)* 6(10), 1813–1825 (2011).
49. Yang M-Q, Zhang N, Xu Y-J. Synthesis of fullerene-, carbon nanotube-, and graphene-TiO₂ nanocomposite photocatalysts for selective oxidation: a comparative study. *ACS Appl. Mater. Interfaces* 5(3), 1156–1164 (2013).

